Quantitative texture analysis of grain-aligned $[Ca_2CoO_3]_{0.62}[CoO_2]$ ceramics processed by the reactive-templated grain growth method

Emmanuel Guilmeau
National Institute of Advanced Industrial Science and Technology, Midorigaoka, Ikeda, Osaka 563-8577, Japan and CRISMAT-ENSICAEN Laboratory, UMR CNRS 6508, 6 Boulevard Maréchal Juin, 14050 Caen Cedex, France

Hiroshi Itahara[a] and Toshihiko Tani
Toyota Central Research and Development Laboratories, Inc., Nagakute, Aichi, 480-1192, Japan

Daniel Chateigner[b] and Dominique Grebille
CRISMAT-ENSICAEN Laboratory, UMR CNRS 6508, 6. Boulevard Maréchal Juin, 14050 Caen Cedex, France

(Received 19 April 2004; accepted 13 October 2004; published online 1 March 2005)

In this study, the texture analysis of highly grain-aligned ceramics of thermoelectric $[Ca_2CoO_3]_{0.62}[CoO_2]$ prepared by the reactive-templated grain growth process was examined. The direct quantitative texture analysis and the combined approach, two advanced methods of x-ray diffraction analysis, were used to analyze fiber texture strength and crystallite size. The calculation of distribution density, correlated to the representation of normal and inverse pole figures, highlights the influence of the texture development on the thermoelectric properties. The electrical conductivity was significantly increased by the improvement of grain alignment during the final uniaxial-pressing treatment. An increase in orientation degree enhances thermoelectric properties, even for highly textured ceramics. The quantitative texture analysis appears to be essential for the development of textured thermoelectric ceramics with enhanced properties. © *2005 American Institute of Physics*. [DOI: 10.1063/1.1829398]

I. INTRODUCTION

The recent discoveries of oxide-based thermoelectric (TE) materials with excellent TE performance, such as $NaCo_2O_4$,[1] $Ca_3Co_4O_9$(Co-349),[2–4] and $Bi_2Sr_2Co_2O_y$,[5,6] aroused a strong interest in materials science. These materials are particularly suited to potential applications in TE power generation as they possess high chemical stability and good TE properties at high temperatures.

The relatively good TE performance and resistance to humidity of Co-349 particularly attracted many researchers dedicated to the improvement of TE properties in TE devices. The substitution of Ca^{2+} by Bi^{3+} and Na^+ has been shown to increase both electrical conductivity (σ) and Seebeck coefficient (S).[7–9] In addition, because the electrical conductivity of Co-349 is strongly anisotropic, with the value along the *ab* plane of the structure around 10 times larger than along the *c* axis at 300 K,[3] some groups reported the preparation of textured Co-349 ceramics by uniaxial pressing of platelike grains[10,11] or by magnetic alignment technique.[12,13] Tani's group proposed notably the reactive-templated grain growth (RTGG) technique using β-$Co(OH)_2$ templates for the fabrication of Co-349 textured ceramics.[14–16] The textured samples show enhanced σ values when compared to the isotropic aggregates.

In particular, the RTGG-prepared Co-349 ceramics exhibit such high orientation degrees that conventional techniques of texture characterization, such as the Lotgering method,[17] are not able to reveal texture differences between them (i.e., Lotgering's factor ~1). Thus, a more effective texture analysis technique is required to determine the optimum preparation conditions. In a previous study,[18] we used a direct quantitative texture analysis to precisely determine the degree of orientation of $(Bi,Pb)_2Sr_2Ca_2Cu_3O_{10+\delta}$ superconductor ceramics. This method, based on the distribution density measurements via the acquisition of several 2θ-scans for various χ angles, presents a real interest to quantitatively determine the fiber texture strength of many materials. Furthermore, for accessing to the complete texture of the material and microstructure informations (crystallite size), the recently developed combined approach has been proved to be a viable tool[19] and was successfully applied to various types of materials.[20–24]

Here, we present the data obtained from x-ray characterization of several TE ceramics using the direct quantitative texture analysis and combined approach. These methods are shown to be highly effective for quantitative texture analysis of cobaltite ceramics, clarifying texture–physical properties relationship for a better understanding and design of improved bulk TE materials.

II. EXPERIMENT

A. Sample preparation

Co-349 ceramic samples were fabricated by the RTGG method, as reported previously.[14,15] Platelike β-$Co(OH)_2$ templates[25] and $CaCO_3$ particles were used as starting powders. These particles were mixed with organic binder and

[a]Electronic mail: h-itahara@mosk.tytlabs.co.jp
[b]Electronic mail: daniel.chateigner@ensicaen.fr

plasticizer in an organic solvent. The slurry was tape casted so that the β-$Co(OH)_2$ platelets were aligned along the casting plane. The obtained tape was stacked, pressed, and then fired in order to remove the organic compounds. After binder removal, the dewaxed body was sintered with uniaxial pressing (UP) at 1193 K in O_2 atmosphere. The sintered samples were prepared by changing pressure and UP duration time: the UP conditions for samples 1, 2, and 3 were set as 9.8 MPa for 2 h, 19.6 MPa for 6 h, and 19.6 MPa for 20 h, respectively.[16]

B. X-ray diffraction analysis

Texture analysis was performed by x-ray diffraction (XRD) using a curved position-sensitive detector (INEL CPS 120) allowing rapid measurement (without Bragg angle scanning) of the whole diffraction pattern at each tilt angle (χ) of the flat sample surface. A 0.5 mm $\times$ 0.5 mm collimated and parallel beam and a small vibration of the sample holder ($\pm$1 mm) were used in order to ensure that all the beam intersected the sample surface even at high sample tilts with a statistically relevant number of irradiated crystallites. Since RTGG-UP ceramics have axially symmetric (fiber) textures (i.e., random in-plane distribution of crystallite *a* and *b* axes), the complete texture analysis is made by measuring the inclination of $\{00\ell\}$ crystallographic planes in terms of the sample surface.[26,27] This was achieved by selecting the (003) reflection using an incidence angle (θ) of 12.5° and scanning the tilt angle from $\chi=0$ to $\chi=60°$, in 5° steps, with an integration time of 1 h for each tilt angle position. The Gaussian integrated (003) peak intensities were normalized into distribution densities (*DD*) by the direct normalization procedure[28] and used as input to reconstruct χ-scans which represent the $\{00\ell\}$ plane dispersions of the crystallites. When no (003) peak was observed even after 1 h of counting time, we assigned zero density values, which happened generally for χ larger than 25°. The maximum of the *DD* (DD_{max}) and its full width at half-maximum (FWHM) were extracted from the χ-scan Gaussian profile and used as parameters for a quantitative appreciation of the crystallite dispersion. For distribution densities, the multiple of a random distribution (m.r.d.)[28] unit is used. A perfectly nonoriented powder exhibits 1 m.r.d. values for all χ (its χ-scan is a straight line), while a textured sample exhibits minima and maxima of densities.

In addition to the direct quantitative texture analysis, we used the combined approach as implemented in the MAUD program package (Materials Analysis Using Diffraction)[29] to analyze texture, crystal structure, and sample microstructures using diffraction spectra. In this approach, the Rietveld method[30] for structure determination is combined with the Williams–Imhof–Matthies–Vinel (WIMV) formalism[31] for the calculation of the orientation distribution function (ODF). The crystallite size determination is obtained after peak deconvolution by applying the Popa formalism.[32] Such texture–structure–microstructure analysis is particularly convenient in our case for the calculation of the ODF and related inverse pole figures, together with crystallite sizes. A calibration of the instrumental contributions to the diffraction profiles for all the scanned positions of the sample was operated on the SRM660 LaB_6 standard from the NIST[33] which served the international round-robin calibration. Accurate structure refinements of these misfit aperiodic phases need a description in the superspace formalism for modulated structures. They were given concerning related polytype phases.[34] From these results, a structural model was built concerning the main phase characterized by the previously reported cell parameters. This model was then confirmed using powder neutron diffraction data[35] and the corresponding structural parameters were then approximately deduced in a commensurate supercell approximant with $b\sim 8b1\sim 13b2$ ($b1$ and $b2$ are *b* parameters of rock-salt-type layer and CoO_2 layer of Co-349, respectively) and a resulting unit cell of $a=4.8309$ Å, $b=36.4902$ Å, $c=10.8353$ Å, and $\beta=98.1317°$. From the ODF, we can determine the texture index F^2, which is an indication of the degree of orientation of the material.[36] Texture components are deduced from the calculated inverse pole figures, where we fix a sample direction and represent the distribution of the associated crystal directions.

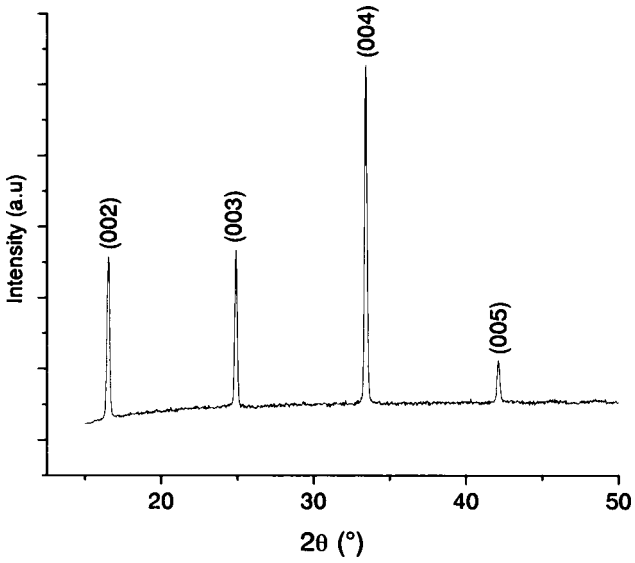

FIG. 1. Typical XRD pattern measured for the surface parallel to the casting plane of sample 1 RTGG-UP ceramic.

C. Thermoelectric properties

For the TE property measurements, a rectangular bar ($2\times4\times10$ mm^3), with the longitudinal direction parallel to the original tape-casting surface, was machined out from the sintered samples. The value of the conductivity along the mean *ab* planes of the oriented polycrystal (σ_{ab}) was measured using a four-probe method with a dc current of 2 mA. The value of S_{ab}, defined as the slope of the relationship between the TE voltage generated between both ends of a bar specimen ΔV and the temperature difference ΔT, was measured at a temperature of 1060 K with ΔT of 1–5 K. The in-plane power factor (PF_{ab}) was calculated from the relationship $PF_{ab}\equiv\sigma_{ab}S_{ab}^2$.

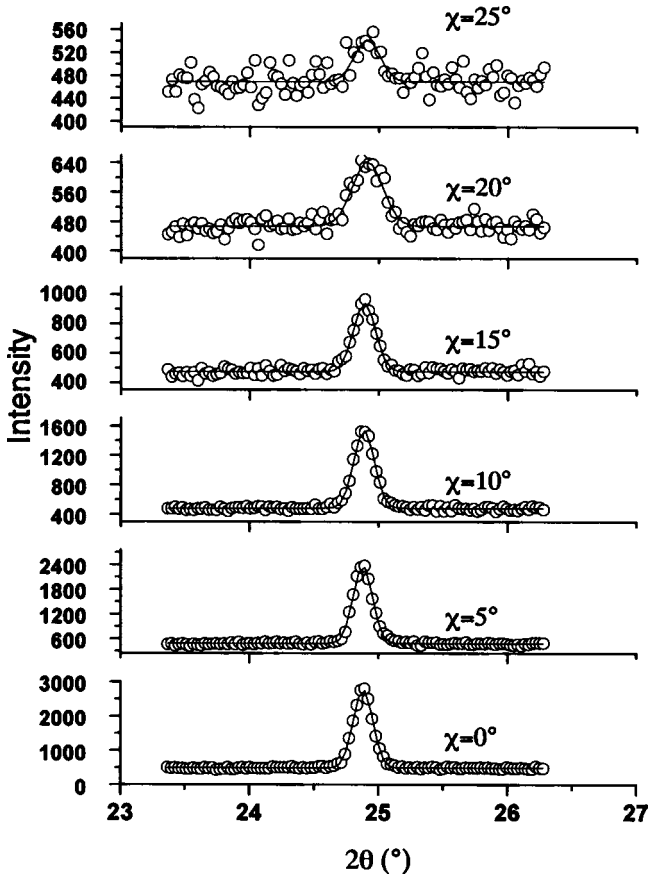

FIG. 2. Experimental and Gaussian fitted profile of the (003) diffraction peak of $[Ca_2CoO_3]_{0.62}[CoO_2]$ for various χ angles (sample 1).

III. RESULTS AND DISCUSSION

A. Direct texture integration

Figure 1 shows the typical XRD pattern measured for the surface parallel to the casting plane of the sintered sample 1. Only 00ℓ peaks were observed, indicating that the $\{00\ell\}$ planes of the Co-349 crystallites are preferentially aligned along the casting plane. In this case, the texture strength of the RTGG-prepared samples cannot be compared to each other using the Lotgering's orientation degree (f) approach, since all the ceramic samples only showed 00ℓ peaks, thereby all exhibiting f values of 1. The evaluation of the texture by f values is restricted to samples showing peaks with nonhomologous $\{hk\ell\}$ planes in the considered experimental range. Furthermore, the f factor does not provide any quantitative information about the angular dispersions of the crystallites.

Consequently, the observation of (003) crystallographic planes for various χ angles (Fig. 2) is necessary to highlight the orientation distribution of c axes from the normal to the casting plane. No more than 5% of the integrated intensity measured at $\chi=0°$ remains at $\chi=25°$ and none for larger χ. After integration and normalization of these peaks, one can represent the distribution of the orientation densities (Fig. 3). A Gaussian shape satisfactorily represents the density distribution profiles for all the ceramic samples with χ angle. The corresponding DD_{max} and FWHM values are summarized in Table I. It is clearly shown that an increase in both pressure and UP duration time induces a texture strength enhancement (decrease of FWHM and increase of DD_{max} values). The obtained texture strengths are in the same range as those obtained in monoclinic crystals having fiber textures like self-supporting clay films.[37]

TABLE I. DD_{max}, FWHM, and texture index (F^2) values for different uniaxial pressures and duration times.

Duration	2 h	6 h	20 h
Pressure (MPa)	*9.8*	*19.6*	*19.6*
DD_{max} (m.r.d.)	*43.5*	*48.7*	*53.0*
FWHM (°)	*21*	*19.9*	*18.5*
Texture index F^2 (m.r.d.^{2})	*7.35*	*26.41*	*32.45*

B. Combined texture–microstructure determination

The analysis of the mean crystallite sizes is possible via the diffraction analysis due to the diffraction peak broadening principally caused by the small size of diffracting domains and the elastic microdistortions. We assumed that no microstrain existed within our samples and extracted the mean crystallite size by the combined analysis. A typical refinement result (for sample 3) is presented in Fig. 4, in which one can appreciate the agreement between the experimental and refined spectra. The reliability corresponds to the texture factors RP and $RP1$ (related to the WIMV refinement) and to Rietveld factors R_w and R_{Bragg} (microstructure Rietveld refinement) equal, respectively, to 9.5%, 9.2%, 5.51%, and 4.43%.

The {003} pole figures (Fig. 5), recalculated from the ODF, exhibit a strong centered pole as a sign of the strong preferential orientation of c axes in the direction perpendicular to the casting plane, as previously seen in the results of the direct normalization procedure (Fig. 3 and Table I). The texture strength evolution showed a similar trend as the results described previously. As the pressure and duration time

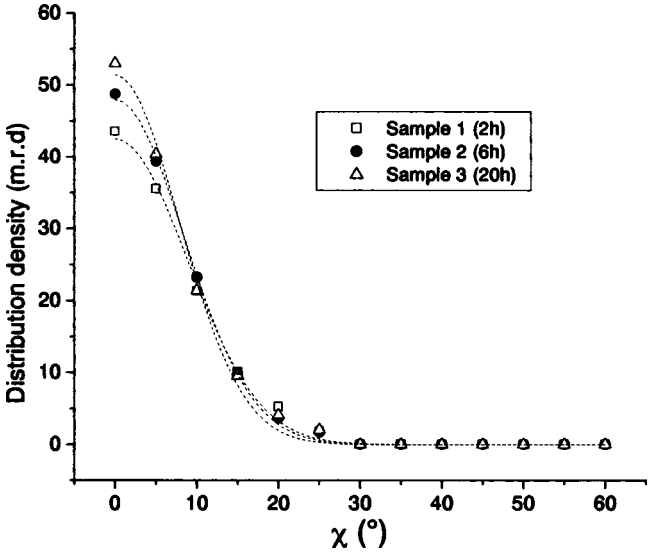

FIG. 3. χ-angle dependence of distribution density for the RTGG-UP samples.

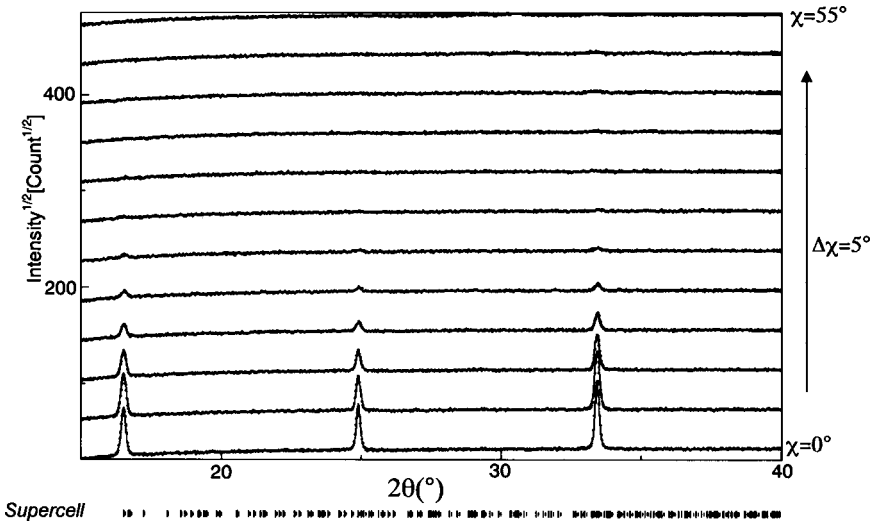

FIG. 4. Experimental and refined XRD patterns at different χ positions for sample 3. Dotted lines represent measured diffraction intensities; solid lines represent fitted curves.

of UP increased, the *c*-axis distribution became sharper, and $DD_{\max}$ values also increased. The texture index F^2, calculated from the ODF, behaves in the same way (Table I). It should be noted that the mean crystallite sizes for samples 1, 2, and 3 were derived from the combined analysis as 1387 ± 16, 1512 ± 15, and 1516 ± 18 Å, respectively. The sizes are increased slightly with increasing pressure and saturated with time. In addition, the grain size and aspect ratio (~5) were unchanged for the current three ceramic samples according to scanning electron microscopy (SEM) observations.[16] Therefore, it is expected that the formation of Co-349 grains on β-$Co(OH)_2$ templates would be completed very quickly, and that the texture improvement might be caused by the rearrangement of platelike Co-349 grains by UP.

The calculated pole figure clarified the texture evolutions. However, a difference of $DD_{\max}$ values is observed between the direct and combined analysis. For the latter analysis, the distribution density at maxima reaches only one-half or one-third of the density calculated from the direct normalization procedure (reported in Table I). This may indicate that the contributions of other minor texture components are overestimated in the combined analysis, whereas they are not considered in the direct analysis. The representation of the inverse pole figure recalculated from the ODF for the direction of the fiber (sample's normal) confirmed this hypothesis by the presence of three components. The inverse pole figure in linear scale [Fig. 6(a)] supports that the major component is related to (00l) planes as same as the result illustrated in the pole figures of Fig. 5. However, the same inverse pole figure expressed in log scale [Fig. 6(b)] indicates the possible existence of two weak minor components; that is, the first and second minor components correspond to $\{0k\ell\}$ and $\{h0\ell\}$ planes parallel to the sample surface, with k/ℓ and h/ℓ ratios close to $8/2-8/3$, and $1/2-1/3$, respectively. An accurate indexation is difficult due to the large number of crystallographic planes in the supercell structure. The appearance of such minor components explains the differences in $DD_{\max}$ observed between the direct and combined approaches. The origin comes from the lack of information at high χ positions due to the beam defocusing, which removes any distinguishable diffracted peaks. This phenomenon, correlated to the incomplete pole-figure coverage, tends to complicate the combined refinement and to lead to incorrect poles such as the minor components appearing in Fig. 6. This has been recently confirmed from a comparative study between x-ray and neutron diffraction. The sample was a Co-349 ceramic textured by the magnetic alignment method and with almost comparable texture strength[26] to the current ceramic samples. The x-ray analysis showed the same phenomenon reported in this paper whereas no parasite poles were observed from neutron analysis. This result can

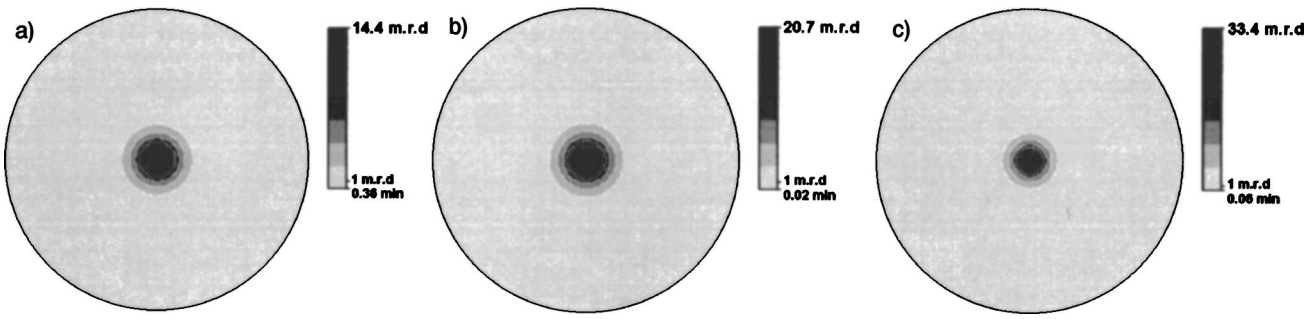

FIG. 5. Calculated (003) pole figures for different uniaxial pressing duration times of (a) 2 h, (b) 6 h, and (c) 20 h; the figures are represented in equal area projections, and linear density scale.

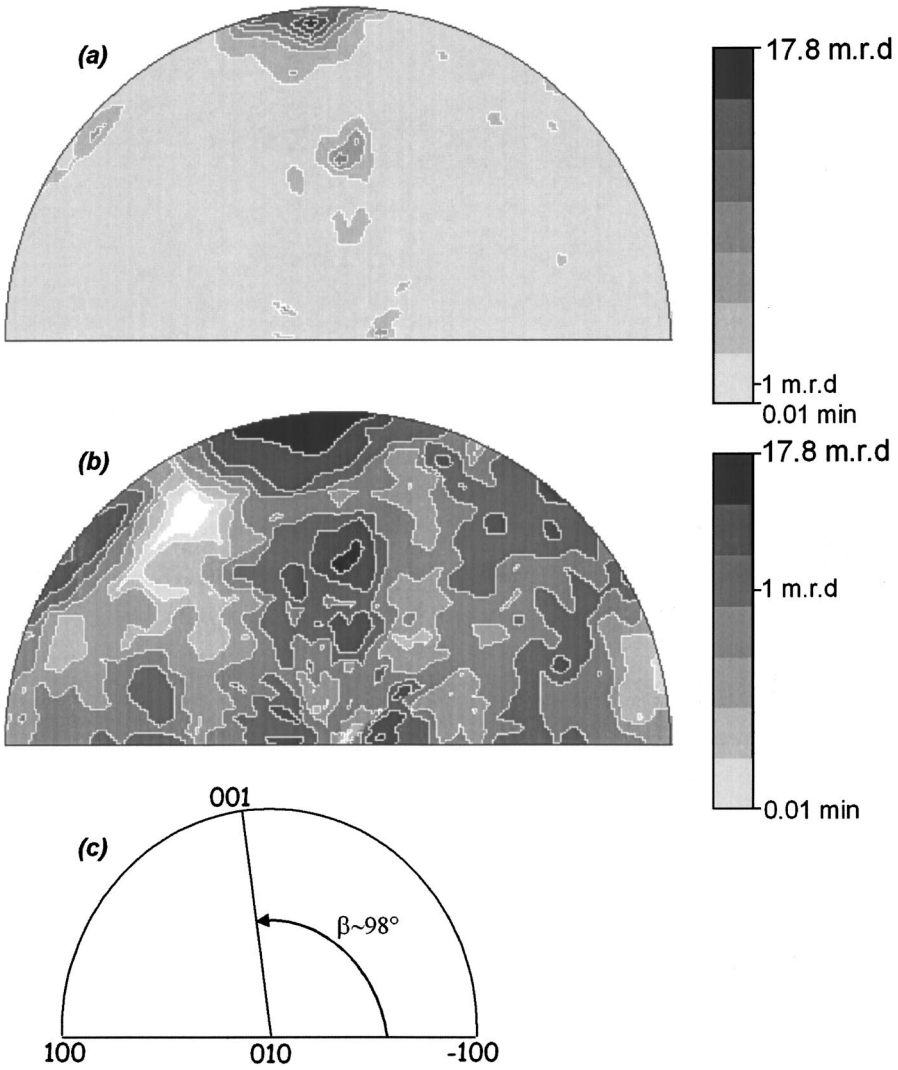

FIG. 6. Calculated inverse pole figures of sample 1 derived from the ODF for the direction normal to the casting plane (fiber axis of the texture). (a) Equal area projections, linear density scale. (b) Equal area projections, logarithmic density scale. (c) Inverse pole figure scheme with crystallographic structure directions.

be explained by the neutron transmission, which avoids the defocusing effect, leading to an accurate representation of the inverse pole figures due to the equivalent diffraction of all (hkℓ) crystallographic planes for each χ orientation. The neutron 2θ patterns exhibit strong diffraction intensities even for χ orientations from 30° to 90°, thereby giving a more accurate refinement due to the increase in structure and texture information when compared to XRD patterns. However, the phenomenon reported in the present article does not affect the comparison of the texture between the three samples. Both the calculated pole figures and inverse pole figures exhibited a clear difference in texture strength among the current three ceramic samples as described earlier.

C. Texture to TE properties correlation

The texture increase is correlated to an enhancement of TE properties (Fig. 7), with larger σ_{ab} and PF_{ab} values for larger pressures and UP duration times. In contrast, the values of S_{ab} are practically unchanged, so that the increase in σ_{ab} is the major contribution to an enhancement of the PF_{ab}. It should be noted that there is not a linear relationship between the texture index and the electrical conductivity, the texture index increasing much more than conductivity in the analyzed range of heat treatment. Such a large texture strength variation (approximately 400% increase) inducing only about 35% of conductivity increase would appear as a rather small effect. Two explanations can be provided to understand this point. Firstly, the texture index is calculated[22,36] by summation of all the squared values of the orientation distribution points. This provides the texture index a large sensitivity to texture increases. Secondly, since mean crystallite and grain sizes do not vary significantly in our samples, one can consider that texture achievement does not influence much the number of grain boundaries in our process. This somehow limits the conductivity increase to only the anisotropy effect.

To establish clearly the importance of texture development on the σ_{ab} values, it is important to clarify microstructural aspects (such as the bulk density, the grain size and related grain boundaries), which have a great influence on the transport properties. The value of σ is reported to proportionally increase with increasing density.[38–40] However, our three samples have similar densities: 4380, 4580, and 4380 kg/m^3 for samples 1, 2, and 3, respectively. The grain size and grain boundary in polycrystalline materials influence the electrical properties due mainly to carriers being scattered by the disordered atom-layers at the grain boundary.[26,41] However, the calculated crystallite sizes were

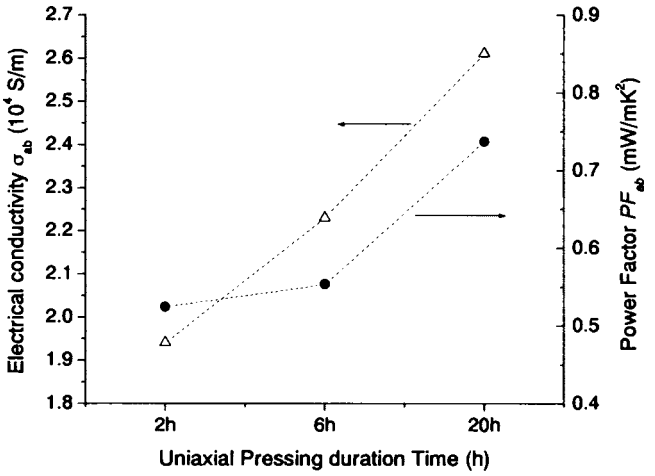

FIG. 7. Uniaxial pressing duration time dependence of electrical conductivity (△) and power factor (●).

respectively similar for our ceramic samples, and SEM study showed that each sample had grains with similar sizes and aspect ratios.[16] Therefore, if grain boundaries can affect the transport properties, it depends only on the texture development and the rearrangement of platelike Co-349 grains by UP. The texture improvement appears here to be the main reason for the increase in σ_{ab} in our ceramic samples. The enhancement of texture would increase the contribution of the conduction path along the *ab* plane with high σ and decrease that along the *c* axis with low σ. The σ_{ab} value of the ceramic increased with increasing orientation degree and reached ~60% of that of single crystal ($\sim 4.35 \times 10^{-4}$ S/m at 973 K).[42] The current texture analysis technique effectively reveals small differences in orientation degree even for highly textured ceramics with $f \sim 1$. This demonstrates its importance in the properties.

IV. CONCLUSION

We conducted quantitative texture analysis for Co-349 ceramics prepared using the RTGG method with different processing parameters (i.e., pressure and duration time of UP). We demonstrated the effectiveness of the texture characterization in explaining the influence of these parameters on TE performance. It was found that enhancement of the σ_{ab} values, induced by the increase in pressure and duration time of UP, correlated to an improvement of the texture strength. The combined texture–structure–microstructure analysis was shown to be highly effective to extract texture strength and crystallite size in a complex misfit crystallographic system. In conclusion, our results reveal the importance of texture analysis in improving understanding and processing design of textured ceramics for potential applications to TE power generation.

ACKNOWLEDGMENTS

Two of the authors (D. C.) and (D. G.) greatly acknowledge the French Ministère de la Recherche et de la Technologie and the Délégation Régionale à la Recherche et à la Technologie-région Basse-Normandie, for financial supports in the x-ray experimentation.

[1] I. Terasaki, Y. Sasago, and K. Uchinokura, Phys. Rev. B **56**, R12685 (1997).
[2] S. Li, R. Funahashi, I. Matsubara, K. Ueno, and H. Yamada, J. Mater. Chem. **9**, 1659 (1999).
[3] A. C. Masset, C. Michel, A. Maignan, M. Hervieu, O. Toulemende, F. Studer, B. Raveau, and J. Hejtmanek, Phys. Rev. B **62**, 166 (2000).
[4] R. Funahashi, I. Matsubara, H. Ikuta, T. Takeuchi, U. Mizutani, and S. Sodeaka, Jpn. J. Appl. Phys., Part 2 **39**, L1127 (2000).
[5] H. Leligny, D. Grebille, O. Perez, A. C. Masset, M. Hervieu, and B. Raveau, Acta Crystallogr., Sect. B: Struct. Sci. **56**, 173 (2000).
[6] R. Funahashi, I. Matsubara, and S. Sodeoka, Appl. Phys. Lett. **76**, 2385 (2000).
[7] S. Li, R. Funahashi, I. Matsubara, K. Ueno, S. Sodeoka, and H. Yamada, Chem. Mater. **12**, 2424 (2000).
[8] G. Xu, R. Funahashi, M. Shikano, I. Matsubara, and Y. Zhou, Appl. Phys. Lett. **80**, 3760 (2002).
[9] M. Mikami, K. Chong, and R. Funahashi (unpublished).
[10] J.-W. Moon, D. Nagahama, Y. Masuda, W.-S. Seo, and K. Koumoto, J. Ceram. Soc. Jpn. **109**, 647 (2001).
[11] R. Funahashi, S. Urata, T. Sano, and M. Kitawaki, J. Mater. Res. **18**, 1646 (2003).
[12] Y. Zhou, I. Matsubara, S. Horii, T. Takeuchi, R. Funahashi, M. Shikano, J. Shimoyama, K. Kishio, W. Shin, N. Izu, and N. Murayama, J. Appl. Phys. **93**, 2653 (2003).
[13] S. Horii, I. Matsubara, M. Sano, K. Fujie, M. Suzuki, R. Funahashi, M. Shikano, W. Shin, N. Murayama, J. Shimoyama, and K. Kishio, Jpn. J. Appl. Phys., Part 1 **42**, 7018 (2003).
[14] T. Tani, H. Itahara, C. Xia, and J. Sugiyama, J. Mater. Chem. **13**, 1866 (2003).
[15] H. Itahara, C. Xia, Y. Seno, J. Sugiyama, T. Tani, and K. Koumoto: Proc. 22nd Int. Conf. Thermoelectrics (ICT2003) (IEEE, Piscataway NJ, 2003) p. 188.
[16] H. Itahara, J. Sugiyama, and T. Tani, Jpn. J. Appl. Phys., Part 1 **43**, 5134 (2004).
[17] F. K. Lotgering, J. Inorg. Nucl. Chem. **9**, 113 (1959).
[18] E. Guilmeau, D. Chateigner, and J. G. Noudem, Supercond. Sci. Technol. **15**, 1436 (2002).
[19] S. Matthies, L. Lutterotti, and H. R. Wenk, J. Appl. Crystallogr. **30**, 31 (1997).
[20] H.-R. Wenk, L. Cont, Y. Xie, L. Lutterotti, L. Ratschbacher, and J. J. Richardson, J. Appl. Crystallogr. **34**, 442 (2001).
[21] M. Morales, D. Chateigner, and D. Fruchart, J. Magn. Magn. Mater. **257**, 258 (2003).
[22] J. Ricote and D. Chateigner, J. Appl. Crystallogr. **37**, 91 (2004).
[23] J.-H. Bae, G. Heo, S. T. Oh, E. Shin, B.-S. Seong, C.-H. Lee, and K. H. Oh, Mater. Sci. Forum **408–412**, 215 (2002).
[24] Y. Xie, H.-R. Wenk, and S. Matthies, Tectonophysics **370**, 269 (2003).
[25] H. Itahara, S. Tajima, and T. Tani, J. Ceram. Soc. Jpn. **110**, 1048 (2002).
[26] E. Guilmeau, D. Chateigner, J. Noudem, R. Funahashi, S. Horii, and B. Ouladiaf, J. Appl. Crystallogr. **38**, 199 (2005).
[27] E. Guilmeau, S. Lambert, D. Chateigner, J. G. Noudem, and B. Ouladiaf, Mater. Sci. Eng., B **104**, 107 (2003).
[28] A. Manceau, B. Lanson, D. Chateigner, J. Wu, D. F. Huo, W. P. Gates, and J. W. Stucki, Am. Mineral. **85**, 133 (2000).
[29] L. Lutterotti, S. Matthies, and H.-R. Wenk, *Textures of Materials*, edited by J. A. Szpunar (NRC Research Press, Ottawa, 1999), Vol. 2, p. 1599.
[30] H. M. Rietveld, J. Appl. Crystallogr. **2**, 65 (1969).
[31] S. Matthies and G. W. Vinel, Phys. Status Solidi B **112**, 111 (1982).
[32] N. C. Popa, J. Appl. Crystallogr. **31**, 176 (1998).
[33] D. Balzar, J. Appl. Crystallogr. **25**, 579 (1992).
[34] S. Lambert, H. Leligny, and D. Grebille, J. Solid State Chem. **160**, 322 (2001).
[35] D. Grebille, S. Lambert, F. Bourée, and V. Petricek, J. Appl. Crystallogr. **37**, 823 (2004).
[36] H. J. Bunge, *Texture Analysis in Materials Science* (Butterworths, London, 1982).
[37] A. Manceau, W. Gates, and D. Chateigner, Phys. Chem. Mater. Treat. **25**, 347 (1998).
[38] W. D. Kingery, H. K. Brown, and D. R. Uhlman, *Introduction to Ceram-*

ics, 2nd ed. (Wiley, New York, 1976), p. 906.
[39]Y. Masuda, D. Nagahama, H. Itahara, T. Tani, W. S. Seo, and K. Koumoto, J. Mater. Chem. **13**, 1094 (2003).
[40]H. Itahara, K. Fujita, J. Sugiyama, K. Nakamura, and T. Tani, J. Ceram. Soc. Jpn. **111**, 227 (2003).
[41]Y. Zhou, I. Matsubara, W. Shin, N. Izu, and N. Murayama, J. Appl. Phys. **95**, 625 (2004).
[42]M. Shikano and R. Funahashi, Appl. Phys. Lett. **82**, 1851 (2003).